Coulomb distortion and medium corrections in nucleon-removal reactions

M. Karakoc[1,4], A. Banu[2], C.A. Bertulani[1], and L. Trache[3]

[1]*Department of Physics & Astronomy,Texas A&M University-Commerce, Commerce, TX 75428*
[2]*Department of Physics & Astronomy,James Madison University,Harrisonburg, VA 22807*
[3]*Cyclotron Institute, Texas A&M University, College Station, Texas 77843, USA and*
[4]*Department of Physics, Akdeniz University, TR-07058 Antalya, Turkey*

Background One-nucleon removal reactions at or above the Fermi energy are important tools to explore the single-particle structure of exotic nuclei. Experimental data must be compared with calculations to extract structure information, evaluate correlation effects in nuclei or determine reaction rates for nuclear astrophysics. However, there is insufficient knowledge to calculate accurately the cross sections for these reactions.

Purpose We evaluate the contributions of the final state interaction (FSI) and of the medium modifications of the nucleon-nucleon interactions and obtain the shapes and magnitudes of momentum distributions. Such effects have been often neglected in the literature.

Method Calculations for reactions at energies 35 - 1000 MeV/nucleon are reported and compared to published data. For consistency, the state-of-the-art eikonal method for stripping and diffraction dissociation is used.

Results We find that the two effects are important and their relative contributions vary with the energy and with the atomic and mass number of the projectile involved.

Conclusions These two often neglected effects modify considerably the one-nucleon removal cross sections. As expected, the effect are largest at lower energies, around 50 MeV/nucleon and on heavy targets.

I. INTRODUCTION

Nucleon knockout reactions in nuclear collisions at and above the Fermi energy in nuclei have become an important tool to determine the occupancy of single-particle states and the correlation effects in the nuclear many-body system (see, e.g. Refs. [1–5]). In peripheral, sudden collisions of fast-moving projectiles with a target nucleus, a single nucleon is removed from the projectile, producing projectile-like residues in the exit channel, which are measured. Referred to the center-of-mass system of the projectile, the transferred momentum is $\mathbf{k}_c$. For the knockout reactions in the sudden approximation, this must equal the momentum of the struck nucleon before the collision. The standard reaction models assume that the ground state of the projectile of spin and parity J^π can be approximated by a superposition of configurations of the form $[I_c^{\pi_c} \otimes nlj]^{J^\pi}$ where $I_c^{\pi_c}$ denote the core states and the nlj are the quantum numbers for the single particle wave functions in a spherical mean field potential. The measured partial cross sections to individual final levels c of the core allow to extract, by comparison with theoretical calculations, the spectroscopic factors for the individual core-single particle configurations. In complete analogy to the use of angular distributions in transfer reactions, the orbital angular momentum l is revealed by the shape of the momentum distributions $P(\mathbf{k}_c)$. It is obvious then that the accuracy of the extracted spectroscopic factors, a measure of the occupancy of the single-particle orbitals in nuclei, and the conclusions that may follow from these spectroscopic factors about correlations inside nuclei depend in direct measure on the accuracy of the cross section calculations. Similarly, the cross sections for one-proton removal reactions $X \to Y + p$ are directly related to the non-resonant part of the astrophysical S-factors for the inverse radiative proton capture Y(p,γ)X (see, e.g., Refs. [4, 6–9]). Again, the results and their reliability depend directly on the reliability and accuracy of the reaction calculations (as discussed in [10]).

The one-nucleon removal cross section is calculated in most reaction models as an incoherent sum of the contributions of all core-single particle configurations making the ground state of the fast moving projectile:

$$\sigma_{-1n} = \sum S(c;nlj)\sigma_{sp}(nlj), \qquad (1)$$

where $S(c;nlj)$ and σ_{sp} are the spectroscopic factors of each configuration and the single particle removal cross section, respectively [4]. A similar relation is valid for momentum distributions. Systematic studies of projectiles and reactions allow the determination of the ordering, spacing and the occupancy of orbitals, essential in assessing how nuclei evolve in the presence of large neutron or proton excess. Much was done in this respect in the last decade in various laboratories. This information can be compared to many-body nuclear structure calculations which are now able to reproduce the measured masses, charge radii and low-lying excited states of a large number of nuclei. It was found that, e.g., for very exotic nuclei, the small additional stability that comes with the filling of a particular orbital can have profound effects upon their existence as bound systems, their lifetime and structure, and lead to the discovery of magic numbers that do not manifest along the valley of stability.

Extensions of the nucleon knockout formalism including the treatment of final-state interactions have been

discussed in Ref. [11] where it is shown that Coulomb final-state interactions are of relevance. In the meantime, inclusion of higher-order effects [12, 13] and a theory for two-nucleon knockout [14–16] have been developed. Knockout reactions represent a particular case for which higher projectile energies allow a simpler theoretical treatment of the reaction mechanism, due to the simplicity of the reaction mechanism and the assumption of a single-step process.

A microscopic approach to direct reactions uses an effective nucleon-nucleon (NN) interaction (e.g. those of Ref. [17]) to start with. This interaction is often used to construct an optical potential with its imaginary part assumed to relate to the real part and its strength adjusted to reproduce experimental data. The real and imaginary parts of the potential can also be independent as in Refs. [6, 7], where the procedure starts from a NN effective interaction with independent real and imaginary parts. For collisions at high energies ($E \gtrsim 100$), it is possible to show that instead of nucleon-nucleon interactions one can use nucleon-nucleon cross sections as the microscopic input [18]. In this case, an effective treatment of Pauli-blocking of nucleon-nucleon scattering is needed, as it manifests through medium modification of nucleon-nucleon cross sections. It is well known that medium modification of the nucleon-nucleon cross sections is necessary for an adequate numerical modeling of heavy-ion collision dynamics in central collisions. In these collisions, the ultimate purpose is to extract information about the nuclear equation of state (EOS) by studying global collective variables describing the collision process. In direct reactions, such as one-nucleon removal reactions, medium effects of NN scattering are smaller because mostly low nuclear densities are probed. A first study of this effect in knockout reactions was carried out in Ref. [19]. Nonetheless, no comparison with experimental data was provided. In this work we explore further consequences of medium corrections and final state interactions in knockout reactions. We study medium effects in the NN cross section in knockout reactions using the methods reported in Ref. [19], namely with a geometrical treatment of Pauli-blocking and with the Dirac-Brueckner theory in terms of baryon densities. We also explore the effect of final state interaction, in particular the effects of Coulomb distortion in the entrance and final reaction channels. This is of relevance as an increasing number of experiments use heavy targets with a large nuclear charge. We compare our results of knockout cross section and momentum distribution calculations to a large number of published experimental data. The purpose is to improve the accuracy of the extracted spectroscopic factors that will lead to better understanding nuclear structure and to check and improve the reliability of the use of one-nucleon removal reactions as indirect methods in nuclear astrophysics.

II. MEDIUM AND DISTORTION EFFECTS

The geometrical treatment of Pauli corrections is performed using the isotropic NN scattering approximation because the numerical calculations can be largely simplified if we assume that the free nucleon-nucleon cross section is isotropic. In this case, a formula which fits the numerical integration of the geometrical model reads [19]

$$\sigma_{NN}(E, \rho_p, \rho_t) = \sigma_{NN}^{free}(E) \frac{1}{1 + 1.892 \left(\frac{2\rho_<}{\rho_0} \right) \left(\frac{|\rho_p - \rho_t|}{\tilde{\rho}\rho_0} \right)^{2.75}}$$

$$\times \begin{cases} 1 - \dfrac{37.02\tilde{\rho}^{2/3}}{E}, & \text{if } E > 46.27\tilde{\rho}^{2/3} \\ \\ \dfrac{E}{231.38\tilde{\rho}^{2/3}}, & \text{if } E \le 46.27\tilde{\rho}^{2/3} \end{cases} \quad (2)$$

where E is the laboratory energy in MeV, $\tilde{\rho} = (\rho_p + \rho_t)/\rho_0$, $\rho_< = \min(\rho_p, \rho_t)$, $\rho_{i=p,t}$ is the local density of nucleus i, and $\rho_0 = 0.17$ fm^{-3}. The parameters and models for the ρ_p and ρ_t densities which have been used to describe the nuclei in this work are presented in Table I.

The Brueckner method goes beyond the simple geometrical treatment of Pauli blocking. Some of the Brueckner results that we used in this analysis have been reported in Refs. [20, 21], where a simple parametrization was given. It reads (the misprinted factor 0.0256 in Ref. [21] has been corrected to 0.00256)

$$\sigma_{np} = \left[31.5 + 0.092 \left| 20.2 - E^{0.53} \right|^{2.9} \right]$$
$$\times \frac{1 + 0.0034E^{1.51}\rho^2}{1 + 21.55\rho^{1.34}},$$
$$\sigma_{pp} = \left[23.5 + 0.00256 \left(18.2 - E^{0.5} \right)^{4.0} \right]$$
$$\times \frac{1 + 0.1667E^{1.05}\rho^3}{1 + 9.704\rho^{1.2}}. \quad (3)$$

The limits of validity of this parametrization are clearly associated with the limits of validity of the Brueckner calculations, which are valid only below the pion-production threshold. A modification of this parametrization was introduced in Ref. [22] and consists in combining the free nucleon-nucleon cross sections parametrized in Ref. [23] with the results of Brueckner theory reported in Refs. [20, 21]. Current theoretical models for the calculation of momentum distributions and cross sections in high-energy nucleon-removal reactions follow a semiclassical probabilistic approach, described, e.g., in Refs. [24, 25]. The method relies on the use of "survival amplitudes" (or S-matrices) in the eikonal approximation,

$$S_i(b) = \exp[i\chi(b)] = \exp\left[-\frac{i}{\hbar v} \int_{-\infty}^{\infty} U_{iT}(\mathbf{r})dz \right], \quad (4)$$

where $r = \sqrt{b^2 + z^2}$, and U_{iT} is the particle(i)-target(T) optical potential. In Ref. [18], a relation has been developed between the optical potential and the nucleon-nucleon scattering amplitude. Such a relation is often

Nuclei	Model	$< r_{ch}^2 >^{1/2}$ (fm)	$< r_m^2 >^{1/2}$ (fm)	a (fm)	α (fm)
(Target)					
[9]Be	HO[a]	2.50(9)	2.367	1.77(6)	0.631
[12]C	HO[b]	-	2.332	1.584	-
(Projectile - Core)					
[10]Be	HO[a]	2.50(9)	2.372	1.77(6)	0.631
[14]N	HO[a]	2.540(20)	2.410	1.729(6)	1.291
[16]B	LDM[c]	-	-	-	-
[22]Mg	HFB[d]	-	2.92	-	-
[23]O	LDM[c]	-	-	-	-
[32]Mg	HFB[d]	-	3.187	-	-

TABLE I: Ground state densities are from Refs. [26, 27, 29–31] where r_{ch} and r_m are root mean square radii of charge and nuclear matter densities, respectively. [a]The nuclear matter densities are obtained using the Harmonic-oscillator (HO) charge densities with parameters a and α from Ref. [26] and the method in Ref. [32]. [b]The HO nuclear matter density is from Ref. [27]. [c]LDM is Liquid Drop Model [28]. [d]Hartree-Fock-Bogoliubov (HFB) calculations are from Refs. [29–31].

referred in the literature as the "t-$\rho\rho$ approximation". The t-$\rho\rho$ approximation is the basis of most calculations of elastic and inelastic scattering involving radioactive nuclei, as experimentally deduced optical potentials are not often available. In this approximation, the eikonal phase becomes

$$\chi(b) = \frac{1}{k_{NN}} \int_0^\infty dq \, q \, \rho_p(q) \, \rho_t(q) \, f_{NN}(q) \, J_0(qb) \ , \quad (5)$$

where $\rho_{p,t}(q)$ is the Fourier transform of the nuclear densities of the projectile and target, and $f_{NN}(q)$ is the high-energy nucleon-nucleon scattering amplitude at forward angles, which can be parametrized as

$$f_{NN}(q) = \frac{k_{NN}}{4\pi} \sigma_{NN} (i + \alpha_{NN}) \exp\left(-\beta_{NN} q^2\right) \ . \quad (6)$$

There are many ways of introducing final state interactions in direct nuclear reactions, some of which are discussed in Refs. [11, 33]. Besides Coulomb repulsion, included by modifying the straight-line trajectories accordingly, we have also modified the integral in Eq. (4) by using the optical potential including the Coulomb potential that modifies the S-matrices according to $S_i = S_i^N \cdot S_i^C$. The Coulomb phase in S_i^C is calculated by assuming a uniform charge distribution with radius R, and is given by

$$\begin{aligned} \chi_C(b) \ = \ & 2\eta \Big\{ \Theta(b - R) \, \ln(kb) \\ & + \ \Theta(R - b) \Big[\ln(kR) + \ln(1 + \sqrt{1 - b^2/R^2}) \\ & - \sqrt{1 - b^2/R^2} - \frac{1}{3}(1 - b^2/R^2)^{3/2} \Big] \Big\} \ , \quad (7) \end{aligned}$$

where Θ is the step function. The value R is chosen to be small enough so that the nuclear S-matrices are basically

zero below $b = R$ because of the strong absorption at small impact parameters.

III. RESULTS AND DISCUSSION

In this section the results for momentum distributions and nucleon-removal cross sections are compared to several experimental data. The focus is the importance of medium corrections of nucleon-nucleon cross sections and of Coulomb distortions. Both effects are expected to decrease as the bombarding energy increases. It is important to include such effects in order to minimize the uncertainty in the extraction of spectroscopic factors, especially at low bombarding energies. To substantiate this assertion, we analyze low energy data on knockout reactions and compare to high energy data. In order to identify the separate contribution of these two factors, we do not vary the geometry of the nucleon binding potentials used to calculate the single particle radial wave functions. That was identified in the literature as another major factor in the calculations, leading to large variations in the extracted spectroscopic factors.

The relevance of medium corrections are motivated by the effect summarized in Figure 1. The cases are shown in Figure 1 are for ^{12}C(^{17}C,^{16}B) at 35 MeV/u, ^{9}Be(^{15}O,^{14}N) at 56 MeV/u, ^{12}C(^{23}Al,^{22}Mg) at 50 MeV/u and ^{9}Be(^{11}Be,^{10}Be) at 60 MeV/u. Later we will discuss more results for each system separately. The dashed and dotted curves show the ratio between the average in-medium and the free nucleon-nucleon cross section as a function of impact parameter (see top scale). We define the average nucleon-nucleon cross section at the distance of closest approach between the projectile and the target using Eq. (2) and the definition

$$\langle \sigma_{NN}(E, b) \rangle = \frac{\int d^3 r_p \, \rho_p(\mathbf{r_p}) \rho_t(\mathbf{r_p} + \mathbf{b}) \, \sigma_{NN}(E, \rho_p, \rho_t)}{\int d^3 r \rho_p(\mathbf{r_p}) \rho_t(\mathbf{r_p} + \mathbf{b})}, \quad (8)$$

where $\mathbf{b}$ is the impact parameter vector, perpendicular to the beam axis.

In Figure 1, the dashed and dotted curves are for core-target and valence nucleon-target average nucleon-nucleon cross sections, respectively. Notice that the target center of mass is located on the right of the top axis scale. Also shown in the figure are the radial wave functions (solid curves) for the valence nucleon-core system and for a few representative reactions considered in this work. For simplicity, in this figure we have used only one of the main configurations for the projectile ground state (more detailed and complete calculations are reported later on in this section). The binding energies "effectively" decrease from the top to low panels. We mention "effectively" because, although the binding energy of the valence proton in ^{23}Al is smaller than for the valence neutron in ^{11}Be, the Coulomb barrier creates an effectively larger binding in ^{23}Al.

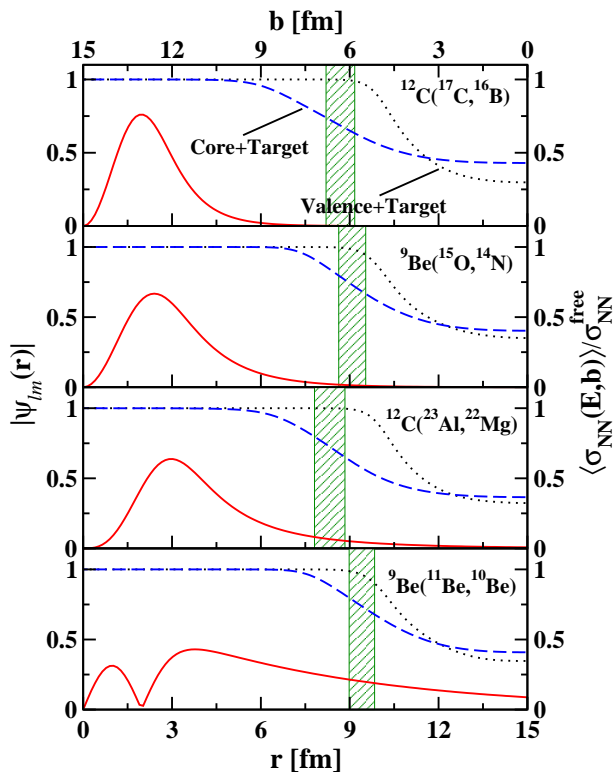It is clearly noticeable from Figure 1 that the wavefunc-

FIG. 1: (Color online). *Top and right scale:* Ratio between average in-medium and the free nucleon-nucleon cross section as a function of the impact parameter. Dashed and dotted curves are for core-target and valence nucleon-target average nucleon-nucleon cross sections, respectively. Notice that the target center of mass is located on the right of the top axis scale. The shaded areas represent the strong absorption radii where the knockout reactions most likely occur and $r_{sa} = b_{sa} = (1.1 \pm 0.1) \, (A_P^{1/3} + A_T^{1/3})$ fm. *Bottom and left scale:* Radial wave functions in arbitrary units (solid curves) for the valence nucleon-core system and for a few representative reactions considered in this work. We have taken only one configuration in cases of systems with multiple configurations.

tions of weakly bound systems extend far within the target where the nucleon-nucleon cross sections are strongly modified by the medium. We have to emphasize that the shaded areas in Fig. 1 are relevant to stress the importance of medium effects at surface region since the reaction is peripheral due to strong absorption at $b < b_{sa}$. Momentum distributions and nucleon removal cross sections in knockout reactions are thus expected to change appreciably with the inclusion of medium corrections of nucleon-nucleon cross section. Such corrections are also expected to play a more significant role for loosely-bound systems.

In the following, we discuss Coulomb corrections. Here we consider the simplest and most straightforward correction one can do, namely the inclusion of a Coulomb phase, which accounts for the distortion of the elastic scattering of the core fragment. It has been usually taken for granted that longitudinal momentum distributions
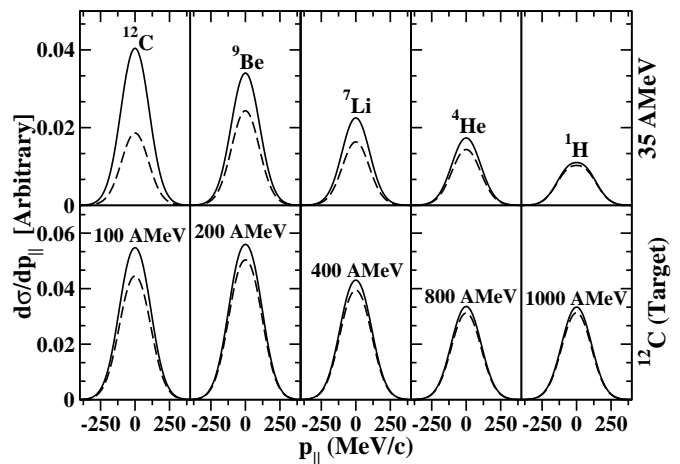

FIG. 2: *Upper panel:* Display of Coulomb scattering effects in longitudinal momentum distributions for the reaction T(^{17}C,^{16}B)X at 35 MeV/u as a function of target T. The solid (dashed) curves are calculations with (without) Coulomb distortion. *Lower panel:* Same as above, but for ^{12}C target and for different beam energies.

are little affected by elastic scattering of the core fragment, the reason being that the longitudinal forces acting on the core fragment reverse sign as the projectile passes by the target, leading to a reduced distortion effect [1]. Further, as has been shown in Ref. [11], the transverse momentum distributions are strongly affected by both nuclear and Coulomb elastic scattering. For heavier targets the distortions are predominantly due to Coulomb repulsion [11]. It is worthwhile mentioning that the implications of the findings on Coulomb distortion effects presented in Ref. [11] have been neglected in the literature. In order to avoid dealing with the effects of the Coulomb scattering, experiments are usually performed with light targets, such as ^{9}Be and relatively high energies, $E \gtrsim 50$ MeV/nucleon. In this work we show that these argumentations are not always valid and need to be studied with care.

As discussed in the previous section, in the presence of the Coulomb field the eikonal S-matrices factorize as the product of the nuclear and the Coulomb contributions: $S(b) = S_n(b)S_C(b)$. Although this does not make any difference for the total stripping cross sections (see Eq. (20) of Ref. [19]), it has an impact on the diffraction dissociation cross section (through the second term of Eq. (21) of Ref. [19]). This means that not only transverse, but also longitudinal momentum distributions will be affected by the Coulomb field. This is shown in Figure 2 for the longitudinal momentum distributions of several systems which we will consider in details later in this section. It is evident from the upper panels of this figure that longitudinal momentum distributions in knockout reactions T(^{17}C,^{16}B)X (and their total cross sections) are strongly influenced by the Coulomb field of the target T at bombarding energies of 35 MeV/nucleon. The solid (dashed) curves are calculations with (without) the inclusion of
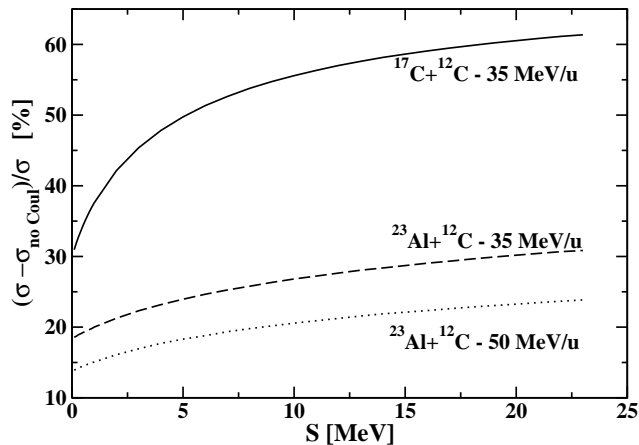
FIG. 3: Total nucleon removal cross sections for the reactions $^{12}C(^{17}C,^{16}B)$ (solid curve) and $^{12}C(^{23}Al,^{22}Mg)$ (dashed curve) at 35 MeV/u. We artificially vary the separation energy S of the proton in ^{17}C and in ^{23}Al. The dotted curve shows the calculation for $^{12}C(^{23}Al,^{22}Mg)$ at 50 MeV/u.

Coulomb scattering. It is also evident that even for the case of light targets, such as ^{9}Be and ^{7}Li, the distributions change appreciably. The lower panels show calculations for the same reaction, but for ^{12}C targets and as a function of the bombarding energy. It is clear that distortions are important even for usually considered "safe" energies, such as 100 MeV/nucleon.

We found that the effect of Coulomb scattering is relatively larger for systems with smaller sizes. This is illustrated in Figure 3 where we present our calculations for the total nucleon removal cross sections for the reactions $^{12}C(^{17}C,^{16}B)$ (solid curve) and $^{12}C(^{23}Al,^{22}Mg)$ (dashed curve) at 35 MeV/u. We artificially vary the binding energy of the proton in ^{17}C and in ^{23}Al. As the separation energy increases so does the percent difference of the cross section, $(\sigma - \sigma_{no\ Coul})/\sigma$, where $\sigma_{no\ Coul}$ is the cross section without the Coulomb scattering phases. With increasing separation energy the relative valence nucleon-core distance decreases and the nucleon removal cross section decreases, but the relative importance of the Coulomb scattering increases. For very small energies the effects of Coulomb dissociation (not considered here) should also become relevant and increase the magnitude of the cross sections. The relative importance of the Coulomb scattering for the removal cross sections decreases with the bombarding energy. This is shown in Figure 3 with the calculation for $^{12}C(^{23}Al,^{22}Mg)$ at 50 MeV/u (dotted curve).

These preliminary discussions support our conclusion that both medium effects and Coulomb distortion play a relevant role in knockout reactions. Next we consider a series of published data for which neither medium or Coulomb corrections were included. We thus quantify the changes in the extracted values of spectroscopic factors in case these effects were to be included in the experimental analysis.

A. $^{12}C(^{23}Al,^{22}Mg)X$ at 50 MeV/u

Recently, the $^{12}C(^{23}Al,^{22}Mg)X$ knockout reaction has been studied at 50 MeV/nucleon to investigate the ground state properties of ^{23}Al [9]. It was shown that the ground-state structure of ^{23}Al is a configuration mixing of a d-orbital valence proton coupled to four core states of ^{22}Mg - 0_{gs}^{+}, 2_{1}^{+}, 4_{1}^{+}, 4_{2}^{+}. The ground state spin and parity of ^{23}Al as $J^{\pi} = 5/2^{+}$ has been confirmed. This experiment had the advantage that exclusive measurements were done and momentum distributions were determined for the four major configurations in the ground state of the projectile (^{23}Al).
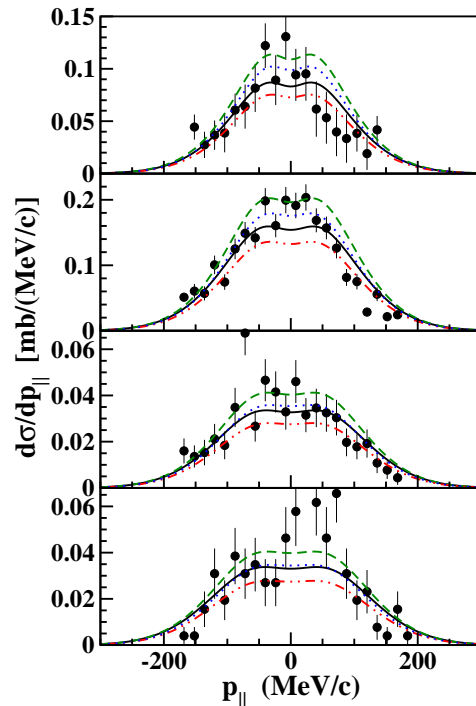

FIG. 4: (Color online). Comparison of experimental data of Ref. [9] and calculations for exclusive longitudinal momentum distributions in the knockout reaction $^{12}C(^{23}Al,^{22}Mg)X$ at 50 MeV/nucleon. The solid line has both Coulomb and medium corrections. The dashed-curve has no medium corrections. The dashed-dotted line includes calculations without Coulomb corrections. The dotted curve neither includes medium effects nor Coulomb corrections.

In this work, we have analyzed the $^{12}C(^{23}Al,^{22}Mg)X$ system to check the relevance of Coulomb and medium effects. The $1d_{5/2}$ wave functions for the valence proton were generated in a spherical Woods-Saxon (WS) potential with the parameters given in Table III.

In the optical limit of the Glauber theory and the t-$\rho\rho$ approximation (explained in detail in Refs. [17, 18]), the eikonal phase is obtained from the input of the nuclear ground state densities and the energy dependent nucleon-nucleon cross sections. The ground state density parameters and models used in this work are shown in Table I, and our results are presented in Fig. 4 and Table

II.

To understand the effects of medium and Coulomb corrections, we have performed the calculations with different inputs. We show in Figure 4 the calculations with both Coulomb and medium corrections (solid curve), calculations without any medium corrections (dashed lines), calculations that exclude Coulomb distortions but keep medium corrections (dashed-dotted curve), and calculations without either Coulomb or medium corrections (dotted curve).

The numerical results for the single particle cross sections with different configurations are shown in Table II. For each of the four configurations - ^{22}Mg - 0_{gs}^+, 2_1^+, 4_1^+, 4_2^+ - the corresponding relative differences between full calculations and calculations without Coulomb corrections are found to be 15%, 17%, 19% and 20%, respectively, whereas between full calculations and calculations without medium corrections the corresponding percentage differences are found to be 24%, 21%, 16% and 13%, respectively.

B. ^{9}Be(^{15}O,^{14}N)X at 56 MeV/u

One-proton removal reaction from ^{15}O on a Be target has been measured at 56 MeV/nucleon and the total knockout cross section is reported as 80±20 mb in Ref. [34]. The authors were able to explain the orbital occupancy of valence protons with a pure $1p_{1/2}$ single particle state using a Glauber reaction model. Their calculations imply that the $1p_{3/2}$ state could also have a small contribution because the calculations with only the $1p_{1/2}$ state yield a narrower momentum distribution than observed in the experiment. The physical implication of this is a possible knockout from more deeply bound protons in the $1p_{3/2}$ state. The contributions from each of the p-states yield spectroscopic factors of 1.27(9) and 0.100(75) for the $1p_{1/2}$ and the $1p_{3/2}$ orbital, respectively (Ref. [34] and references therein).

We have followed the interpretation of Ref. [34] and calculated the one-proton removal cross sections for the same reaction with the same orbital occupancy assumption. The parameters are shown in Tables III and I. Our calculations with both Coulomb and medium corrections by slightly changing the spectroscopic factors as 1.42 and 0.13 are in agreement with the results of Ref. [34]. The calculated one-proton removal cross sections are 78.79 mb, 75.20 mb, 93.98 mb and 90.74 mb with both Coulomb and medium corrections, no Coulomb corrections, no medium corrections and neither medium effects nor Coulomb corrections, respectively. The difference between full calculations, including medium and Coulomb scattering effects, and calculations without Coulomb corrections is of the order of 5%, and between full calculations and calculations without medium effects is nearly 19%. This is remarkable even though it fits again within the error of the total knockout cross section experimental data. We thus conclude that for this case, medium
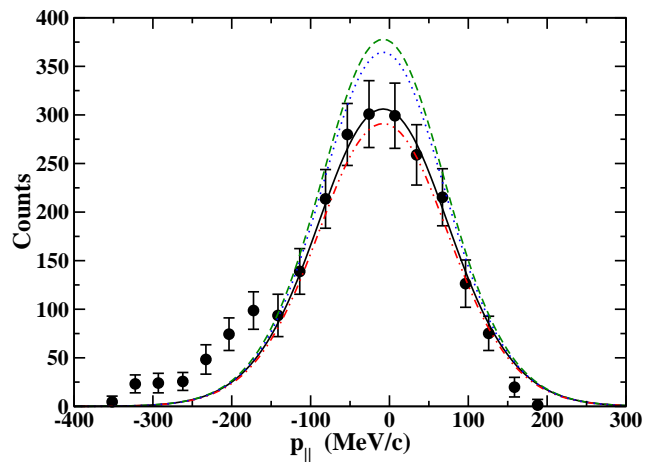

FIG. 5: (Color online) Longitudinal momentum distributions for the ^{9}Be(^{15}O,^{14}N)X reaction at 56 MeV/u. Solid lines represent calculations that include both Coulomb and medium corrections. Dashed lines stem from calculations that do not include medium corrections. Calculations denoted by dashed-dotted curves are performed without Coulomb corrections. The dotted curve does not include medium effects nor Coulomb corrections. The data are taken from Ref. [34].

effects and Coulomb distortion do not have a sizable impact on the extraction of spectroscopic factors. However, one can easily see from Fig. 5 that the data shows an asymmetry which can only be explained with inclusion of higher-order effects in the reaction mechanism. Distortions will be manifest due to continuum-continuum coupling of states involving the interaction of core with the valence proton. These mechanisms have not been considered in the present work.

C. ^{12}C(^{17}C,^{16}B)X at 35 MeV/u

1. Transverse momentum distributions

One-proton removal reaction from ^{17}C, with a separation energy of 23 MeV, has been measured in the reaction ^{12}C(^{17}C,^{16}B)X at 35 MeV/nucleon with the goal to understand the low-lying structure of the unbound ^{16}B nucleus. Using this reaction, Ref. [35] studied the unbound ^{15}B+n system with the assumption of a d-wave neutron decay. Our interest is to compute the transverse momentum distribution of the ^{16}B fragment following the same assumptions as in Ref. [35] in order to study the consequences of medium and Coulomb corrections. The configuration of the proton removed from ^{17}C is assumed to be

$$\begin{aligned}
|^{17}\text{C}\rangle = &\; \alpha_1 |^{16}\text{B}(0^-) \otimes \pi 1p_{3/2}\rangle \\
&+ \alpha_2 |^{16}\text{B}(3_1^-) \otimes \pi 1p_{3/2}\rangle + \alpha_3 |^{16}\text{B}(2_1^-) \otimes \pi 1p_{3/2}\rangle \\
&+ \alpha_4 |^{16}\text{B}(2_2^-) \otimes \pi 1p_{3/2}\rangle + \alpha_5 |^{16}\text{B}(1_1^-) \otimes \pi 1p_{3/2}\rangle \\
&+ \alpha_6 |^{16}\text{B}(3_2^-) \otimes \pi 1p_{3/2}\rangle,
\end{aligned} \tag{9}$$

Configuration	E_x [keV]	$\sigma_{sp}(nlj)$ [mb]			
		Full	no medium	no Coulomb	Free
$^{22}\text{Mg}(0_{gs}^+) \otimes \pi 1d_{5/2}$	0	27.1	33.8	23.2	30.1
$^{22}\text{Mg}(2_1^+) \otimes \pi 1d_{5/2}$	1247	23.7	28.7	19.9	25.1
$^{22}\text{Mg}(4_1^+) \otimes \pi 1d_{5/2}$	3308	20.4	23.9	16.7	20.4
$^{22}\text{Mg}(4_2^+) \otimes \pi 1d_{5/2}$	5293	18.4	21.0	14.8	17.6

TABLE II: Single particle cross sections are shown for each case separately.

J_π	V_0 (MeV)	r_0 (fm)	a_0 (fm)	V_{s0} (MeV)	r_{s0} (fm)	a_{s0} (fm)	r_c (fm)	S_{eff} (MeV)
$\lvert ^{10}\text{Be}(J^\pi) \otimes \nu 2s_{1/2} \rangle$								
$0_{(g.s)}^+$	61.13	1.21	0.52	-	-	-	1.21	0.504
$\lvert ^{14}\text{N}(J^\pi) \otimes \pi nlj \rangle$								
$1_{(g.s)}^+(1p1/2)$	48.36	1.19	0.60	-	-	-	1.19	7.297
$1_{(g.s)}^+(1p3/2)$	48.36	1.19	0.60	-	-	-	1.19	7.297
$\lvert ^{16}\text{B}(J^\pi) \otimes \pi 1p_{3/2} \rangle$								
$0_{(g.s)}^+$	79.46	1.09	0.50	35.0	1.09	0.50	1.09	23.330
3_1^-	80.35	1.09	0.50	35.0	1.09	0.50	1.09	23.979
2_1^-	80.75	1.09	0.50	35.0	1.09	0.50	1.09	24.273
2_2^-	81.85	1.09	0.50	35.0	1.09	0.50	1.09	25.078
1_1^-	82.17	1.09	0.50	35.0	1.09	0.50	1.09	25.318
3_2^-	79.93	1.09	0.50	25.0	1.09	0.50	1.09	26.066
$\lvert ^{22}\text{Mg}(J^\pi) \otimes \pi 1d_{5/2} \rangle$								
$0_{(g.s)}^+$	54.60	1.18	0.60	5.0	1.18	0.60	1.18	0.141
2^+	56.96	1.18	0.60	5.0	1.18	0.60	1.18	1.388
4_1^+	60.67	1.18	0.60	5.0	1.18	0.60	1.18	3.449
4_2^+	64.07	1.18	0.60	5.0	1.18	0.60	1.18	5.434
$\lvert ^{23}\text{O}(J^\pi) \otimes \nu 2s_{1/2} \rangle$								
$1/2_{(g.s)}^+$	42.40	1.27	0.70	-	-	-	1.27	3.610
$\lvert ^{32}\text{Mg}(J^\pi) \otimes \nu nlj \rangle$								
$0_{(g.s)}^+(1d_{3/2})$	-	-	-	-	-	-	-	2.21
$3^-(2p_{3/2})$	79.92	1.04	0.70	10.0	1.03	0.70	1.04	5.07
$3^-(1f_{7/2})$	86.63	1.04	0.70	10.0	1.03	0.70	1.04	5.07
$2_2^+(2s_{1/2})$	51.55	1.04	0.70	10.0	1.03	0.70	1.04	5.22

TABLE III: Bound state potential parameters for the systems studied in the present work. r_0, r_{s0} and r_c are the reduced radius of the bound state potentials where $r_i = R_i/A_p^{1/3}$ ($i = 0, s0, c$). S_{eff} is effective separation energy: $S_{eff} = S_i + E_x^{core}$ where $i = proton$ or $neutron$ and E_x^{core} is core excitation energy.

where α_i is the spectroscopic amplitude for a core-single particle configuration $i = (c \otimes nlj)$.

Using spectroscopic factors obtained by means of a shell-model calculation with the WBP interaction [36], Ref. [35] obtained a good agreement between data and calculated transverse momentum distributions. But the measured total cross section is 6.5(1.5) mb against a theoretical result of 24.7 mb. The explanation of this large difference is proposed in Ref. [37] as a reduction of the spectroscopic factor by 70% for strongly bound nucleon systems. After this spectroscopic reduction is accounted for, the theoretical estimates for the cross section becomes 7.5 mb, in reasonable accordance with the data.

In the present work, we do not elaborate on the assumption introduced in Ref. [35], and we use the same configuration and spectroscopic factors as in [35]. The proton binding potential parameters are shown in Table III which are adjusted to obtain the effective separation energies. The ground state densities are also listed in Table I. Here, as it is shown in Figure 6, we find that medium corrections change the total knockout cross sections by 5%, but the Coulomb corrections have a very large effect which is almost 60% between calculations with Coulomb and without Coulomb distortion. The reason for this difference is that the Coulomb distortion and repulsion effectively increases the collision distance at the small impact parameters needed to remove a strongly bound nucleon. This was not observed in the previous case ($^9\text{Be}(^{15}\text{O},^{14}\text{N})\text{X}$ at 56 MeV/u) because of the small nuclear binding in that case. We have also observed that this effect sharply reduces the calculated cross sections and the removal is more effective as
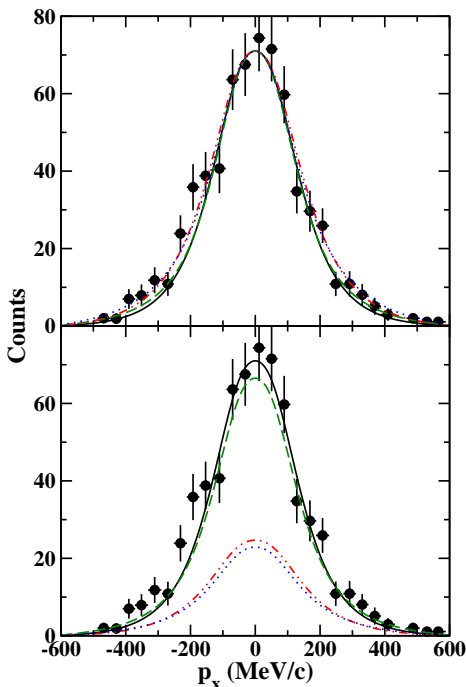
FIG. 6: (Color online). Transverse momentum distributions for the ^{12}C(^{17}C,^{16}B)X system at 35 MeV/u. Solid lines represent calculations including both Coulomb and medium corrections. Dashed lines stem from calculations that do not include medium corrections. Calculations represented by dashed-dotted curves are performed without Coulomb corrections. The dotted curve does not include medium effects nor Coulomb corrections. The data are taken from Ref. [35]. *Top panel:* One can see that, when properly scaled, all four curves from the calculations reproduce the shape of the momentum distributions. *Bottom panel:* The relative differences of our results are illustrated when the full calculation (solid line) is scaled to the data.

the bombarding energy decreases.

2. *Longitudinal momentum distributions*

We have made a more systematic analysis to understand the reason of the effect discussed in the previous subsection. We have observed that the strong dependence on Coulomb distortions are also present in longitudinal momentum distributions. It has long been thought that longitudinal momentum distributions are free from uncertainties related to the knowledge of the optical nucleus-nucleus potentials when compared to the transverse distributions. This was first shown in Ref. [1]. Here we report calculations for the same $|^{16}\mathrm{B}(0^-) \otimes \pi 1p_{3/2}\rangle$ configuration, with the same parameters and ground state densities, as discussed in the previous subsection. We find that although the Coulomb distortions create a similar effect for this particular knockout reaction on both transverse and longitudinal momentum distributions as can be seen in Fig. 2, the effect on transverse

momentum distributions is bigger than the corresponding one for longitudinal momentum distributions by about 5%. This is expected on physics grounds. Nonetheless, such a large effect on longitudinal momentum distributions was not initially anticipated. By comparison with other cases, we found that this large effect is due to the low bombarding energy in this particular reaction combined with a large binding energy of the projectile. This interpretation is also as it is validated by inspection of Figs. 2 and 3.

The source of this difference stems from the diffraction dissociation contribution to the cross sections. To substantiate our claim, we have looked at the details of the knockout cross section which has two parts for the production of a given final state of the residue. The most important of the two, commonly referred to as stripping or inelastic breakup, represents all events in which the removed nucleon reacts with and excites the target from its ground state. The second component, called diffractive or elastic breakup [38], represents the dissociation of the nucleon from the residue through their two-body interactions with the target, each being elastically scattered. We notice that the total stripping cross section is given by [11]:

$$\sigma_{\mathrm{str}} = S(c; nlj)\frac{2\pi}{2l+1} \sum_m \int_0^\infty db_n \, b_n \, \left[1 - |S_n(b_n)|^2\right]$$
$$\times \int d^3r \, |S_c(b_c)|^2 |\psi_{lm}(\mathbf{r})|^2, \qquad (10)$$

whereas the integrated diffraction dissociation cross section is given by [33]:

$$\sigma_{\mathrm{dif}} = S(c; nlj)\frac{2\pi}{2l+1} \sum_m \int_0^\infty db_n \, b_n$$
$$\times \left\{ \int d^3r \left| S_n(b_n) S_c(b_c) \psi_{lm}(\mathbf{r}) \right|^2 \right.$$
$$\left. - \sum_{m'} \left| \int d^3r \psi_{lm'}(\mathbf{r}) S_c(b_c) S_n(b_n) \psi_{lm}(\mathbf{r}) \right|^2 \right\} \quad (11)$$

One can see from these expressions that the stripping cross sections are not affected by the Coulomb distortions because this distortion is manifest through a real phase in the eikonal S-matrices calculated in the Glauber approximation. The magnitude of the cross sections are therefore not changed, as the square of the S-matrices entering Eq. (10) are only changed by the imaginary part of the potential entering Eq. (4). On the other hand, the second term of the diffraction dissociation cross sections in Eq. (11) is appreciably modified by the Coulomb phase factor. As seen from Figure 2, the effect gets smaller with decreasing target atomic number because the Coulomb phase increases, or when the beam energy increases because then the Coulomb recoil becomes irrelevant.
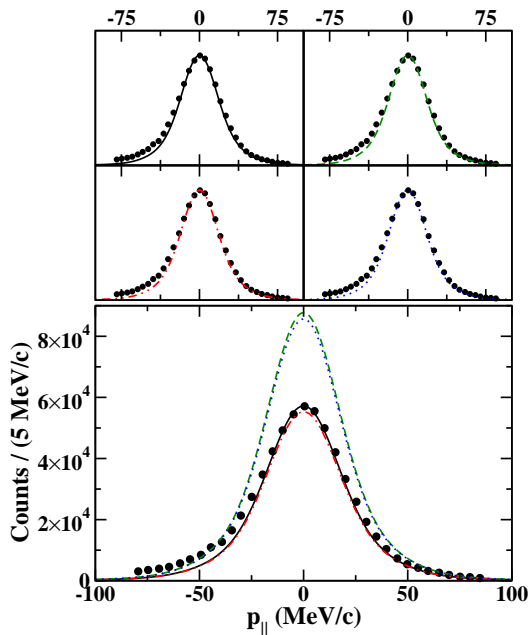
σ_{-1n}	^{12}C(^{17}C,^{16}B)			^{9}Be(^{11}Be,^{10}Be)		
$= \sigma_{dif} + \sigma_{str}$	Full	no Coul	no med	Full	no Coul	no med
Strip. [mb]	7.10	7.10	5.09	126.5	126.5	169.7
Diff. [mb]	18.63	2.42	19.39	52.8	46.7	104.8
Total [mb]	25.74	9.52	24.48	179.3	173.2	274.5

TABLE IV: The cross sections calculated for the systems, ^{12}C(^{17}C,^{16}B) at 35 MeV/nucleon and ^{9}Be(^{11}Be,^{10}Be) at 60 MeV/nucleon.

to the target where the Coulomb interaction is larger. The evidence of this can be seen in Table IV. It is thus clear why medium and Coulomb corrections are more important in the ^{9}Be(^{11}Be,^{10}Be) and the ^{12}C(^{17}C,^{16}B) cases, respectively.

E. ^{12}C(^{24}O,^{23}O)X at 920 MeV/u

The momentum distribution of the one-neutron removal residues from the ^{12}C(^{24}O,^{23}O)X reaction was measured for the first time at 920 MeV/nucleon and reported in Ref. [40]. The data could be explained with a spectroscopic factor S=1.74(19) of an almost pure $2s_{1/2}$ single-particle state for the valence neutron. This work, together with recent theoretical calculations, suggests that ^{24}O is a newly discovered doubly magic nucleus. The one-neutron removal cross section was found to be 63(7) mb. The calculations in Ref. [40] were based on a few-body Glauber formalism [41] for two configurations: (a) ^{23}O$_{gs}$(1/2$^+$) + n in $2s_{1/2}$ orbital and (b) ^{23}O$_{gs}$(5/2$^+$) + n in $1d_{5/2}$ orbital. The wave functions for the configurations are obtained with a Woods-Saxon potential by adjusting the depth of the potential to reproduce the one-neutron separation energy S_n=3.61(27) MeV [29]. Using a pure $2s_{1/2}$ configuration with S=1 leads to a cross section of 34 mb. The calculation is in agreement with the data when it is multiplied by S=1.74(19). This large spectroscopic factor indicates that the single-particle strength of the valence neutron is strongly weighted in the $2s_{1/2}$ state.

In the present work we have reproduced the data of Ref. [40] also by assuming a $2s_{1/2}$ orbital only. The potential parameters for the bound state wave function are given in Table III and the ground state density for the ^{23}O$_{gs}$ core is obtained using liquid droplet model (LDM) densities [42], as indicated in Table I. To understand the differences between medium effect models, four different calculations including Coulomb corrections have been made for this system. The calculated one-neutron removal cross sections are 58.58 mb, 54.08 mb, 78.74 mb and 53.25 mb using free [19], Pauli corrected (Eq. 2), Brueckner (Eq. 3) and phenomenological parameterizations [22] of the nucleon-nucleon cross sections, respectively. Except for the result obtained with the Brueckner theory, they are all in agreement with the previous work and with the data. The relative difference between the re-

FIG. 7: (Color online). Longitudinal momentum distributions of for the reaction ^{9}Be(^{11}Be,^{10}Be) at 60 MeV/nucleon. Solid lines represent calculations that include both Coulomb and medium corrections. Dashed lines stem from calculations that do not include medium corrections. Calculations denoted by dashed-dotted curves are performed without Coulomb corrections. The dotted curve does not include medium effects nor Coulomb corrections. The data is taken from Ref. [39]. *Top panel:* One can see that, when properly scaled, all four curves from the calculations reproduce the shape of the momentum distributions. *Bottom panel:* The relative differences of our results are illustrated when the full calculation (solid line) is scaled to the data.

D. ^{9}Be(^{11}Be,^{10}Be)X at 60 MeV/u

In order to further understand the dependence of the Coulomb distortion on the nuclear binding, we consider the reaction ^{9}Be(^{11}Be,^{10}Be)X at 60 MeV/u which can be modeled by a core plus valence system with the assumption ^{10}Be$_{gs}$(0$^+$) + n in $2s_{1/2}$ orbital for the ground state of ^{11}Be$_{gs}$(1/2$^+$) ($S_n = 0.504$ MeV). Here we use the same Woods-Saxon potential parameters for the bound state as published in Ref. [25]: ($R_0 = 2.70$ fm, $a_0 = 0.52$ fm). In Figure 7 and Table IV we present our results for the neutron removal longitudinal momentum distribution of 60 MeV/nucleon ^{11}Be projectiles incident on ^{9}Be targets.

It is evident from Fig. 1 that ^{17}C has the smallest "effective" size and that ^{11}Be has the biggest size among the low energy systems in this study. The nuclear size is important for low energy cases because the diffraction dissociation becomes dominant when the nuclear size is smaller, but the stripping becomes dominant when the nuclear size is bigger. The reason for this is that a large projectile feels the nuclear interaction already at large impact parameters. A small projectile can come closer

sults obtained using Brueckner corrections and with free nucleon-nucleon cross sections is about 34%. However, we do not consider a real discrepancy, as the Brueckner parametrization have been extrapolated well beyond their validity. Brueckner calculations are limited by the pion-production threshold, and should only be valid for projectile energies below 300 MeV/nucleon.

Thus we verify that the experimental data for the reaction ^{12}C(^{24}O,^{23}O)X at 920 MeV/u is well reproduced with the use of free nucleon-nucleon cross sections. The changes introduced by Pauli-blocking with the geometric model are small, and the phenomenological account of medium effects at this high energy also basically agree with the results using free cross sections.
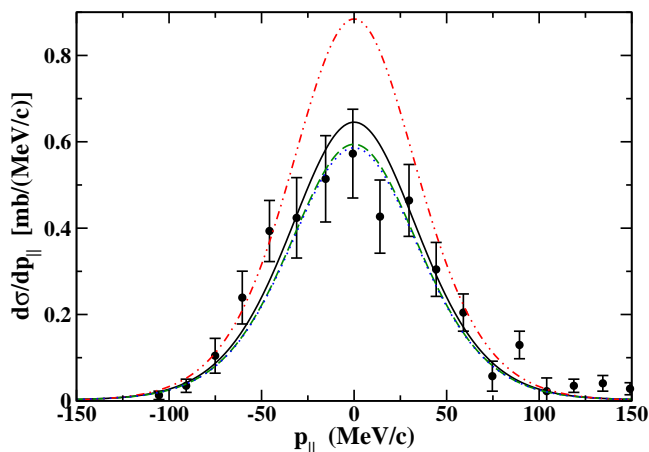
F. ^{12}C(^{33}Mg,^{32}Mg)X at 898 MeV/u

FIG. 8: (Color online). The longitudinal momentum distributions for ^{12}C(^{24}O,^{23}O)X reaction at 920 MeV/nucleon. The curves are calculated with the free NN cross sections (solid), with a geometrical account of Pauli blocking (dashed), a phenomenological fit from Ref. [22] (dotted), and a correction from Brueckner theory (dashed-dotted). The data has been taken from Ref. [40].

The ground state structure of ^{33}Mg, a nucleus belonging to the $N = 20$ island of inversion, has been studied in Ref. [43] by means of nucleon-removal reactions on a carbon target at 898 MeV/nucleon. The longitudinal momentum distribution of the ^{32}Mg core was measured and the one-neutron removal cross section was found to be 74(4) mb. Most of the contribution to the ground state structure of ^{33}Mg was shown to arise from the $2p_{3/2}$ orbital.

The longitudinal momentum distribution obtained in Ref. [43] cannot be reproduced with a pure single particle state. It has been discussed in details in Ref. [43] the reason why a configuration mixing of different single-particle states is needed. Two different configuration mixings for

the ground state of ^{33}Mg were assumed. The first one is

$$|^{33}\text{Mg}_{gs}(3/2^-)\rangle =$$
$$\alpha_1|^{32}\text{Mg}(2_1^+) \otimes \nu 2p_{3/2}\rangle + \alpha_2|^{32}\text{Mg}(1^-) \otimes \nu 2s_{1/2}\rangle$$
$$+ \alpha_3|^{32}\text{Mg}(2_1^+) \otimes \nu 1f_{7/2}\rangle + \alpha_4|^{32}\text{Mg}(1^-) \otimes \nu 1d_{3/2}\rangle$$
$$+ \alpha_5|^{32}\text{Mg}(gs) \otimes \nu 2p_{3/2}\rangle \qquad (12)$$

and the second is

$$|^{33}\text{Mg}_{gs}(3/2^+)\rangle = \alpha_1|^{32}\text{Mg}(3^+) \otimes \nu 2p_{3/2}\rangle$$
$$+ \alpha_2|^{32}\text{Mg}(2_2^+) \otimes \nu 2s_{1/2}\rangle + \alpha_3|^{32}\text{Mg}(3^+) \otimes \nu 1f_{7/2}\rangle$$
$$+ \alpha_4|^{32}\text{Mg}(gs) \otimes \nu 1d_{3/2}\rangle, \qquad (13)$$

where α_i are the spectroscopic amplitudes for each single-particle orbital. The values of the corresponding spectroscopic factor S_i were found by χ^2 minimization and their values for the second configuration are $S_1 = 2.2^{+0.2}_{-0.5}$, $S_2 = 0.1^{+0.0}_{-0.1}$, $S_3 = 1.1^{+0.1}_{-0.5}$ and $S_4 = 0.0^{+0.5}_{-0.0}$ [43].
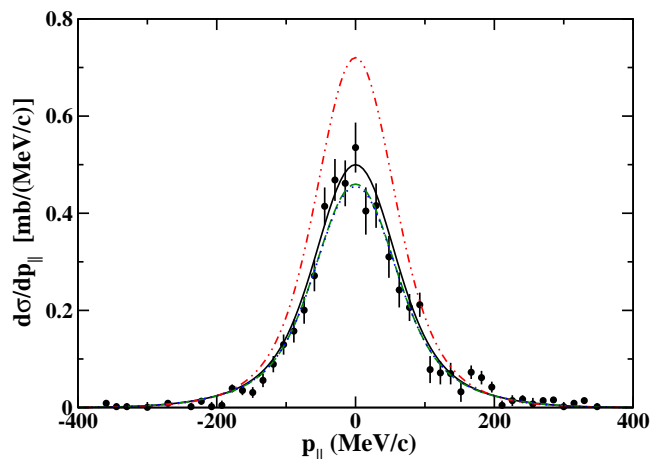

FIG. 9: (Color online). The inclusive longitudinal momentum distributions for the ^{12}C(^{33}Mg,^{32}Mg)X system at 898 MeV/nucleon. The data has been taken from R. Kanungo et al. [43]. The curves are calculated with the free NN cross sections (solid), with a geometrical account of Pauli blocking (dashed), a phenomenological fit from Ref. [22] (dotted), and a correction from Brueckner theory (dashed-dotted).

In our calculations we have chosen the second configuration set used in Ref. [43], Eq. 13, since the ^{33}Mg ground state is usually accepted to be $J^\pi = 3/2^+$. We apply the same procedure as described before to obtain bound state wave functions and eikonal phases. The parameters for the bound state potentials and ground state densities are shown in Table III and Table I, respectively. We have used nearly the same spectroscopic factors within the error bar range of Ref. [43] to make a consistent comparison of the medium effects. Our results yield a small but relevant variation of the one-neutron removal cross sections using the free, Pauli corrected, and phenomenological NN cross sections, namely 83.70 mb, 77.90 mb, and 77.63 mb, respectively. As observed in the case of the ^{12}C(^{24}O,^{23}O)X at 920 MeV/u, the use of
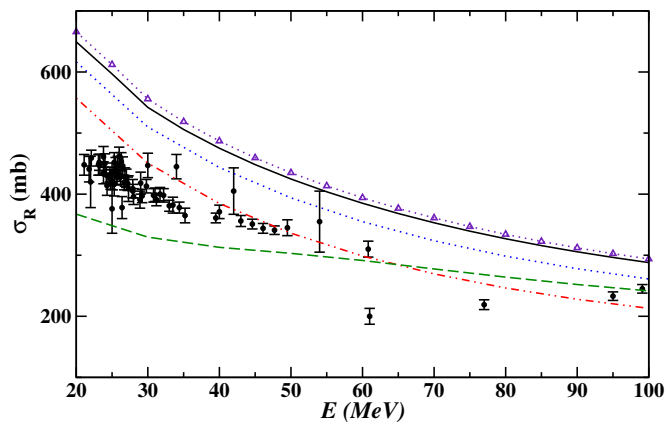
FIG. 10: (Color online). The total reaction cross section of the p + ^{12}C taken from Ref. [44]. The curves are calculated with the free NN cross sections from Ref. [45] (solid), with a geometrical account of Pauli blocking (dashed), a phenomenological fit from Ref. [22] (dotted), and a correction from Brueckner theory (dashed-dotted). The triangle-dotted curve is calculated with the same free NN cross sections from Ref. [45], but with an another HFB calculation [46] for the ^{12}C ground state density.

Brueckner corrected NN cross sections yields 112.92 mb, about 35% relative to the calculations using the free NN cross sections. For the same reason as with the previously considered reaction, this discrepancy is meaningless as one extrapolates the Brueckner results beyond their regime of validity.

Both reactions considered above are very illustrative as they show a great consistency between the calculations performed by different authors, with somewhat different methods. They also show the expected relevance of medium corrections at intermediate and low energy collisions.

G. Relevance of medium effects

As we mentioned above, medium effects have been routinely neglected in the experimental analysis of knockout reactions. But their relevance has been known for a long time in the analysis of elastic and inelastic scattering, as well as of total reaction cross sections [17, 18]. The effects are larger at lower bombarding energies, where Pauli blocking strongly reduces the nucleon-nucleon cross sections in the medium. A systematic study of these effects has been presented in Ref. [18].

To corroborate these statements, in figure 10 we show the data on p + ^{12}C reaction cross sections taken from the Ref. [44] in the energy region of our interest, 20-100 MeV/nucleon. The cross sections were calculated from the relation

$$\sigma_R = 2\pi \int db \; b \left[1 - |S(b)|^2 \right], \qquad (14)$$

where $S(b)$ has been calculated using Eqs. (4,5,6) and the carbon matter density from a Hartree-Fock-Bogoliubov calculation [46]. Several distinct calculations are shown. The solid curve uses Eq. (5) with the free nucleon-nucleon cross sections and the carbon matter density from a HFB calculation [47], whereas the triangle-dotted curve (the triangles are not data, but used for better visibility) uses a different HFB density [46], consistent with the calculations presented in Ref. [48]. As expected, that the agreement between the two calculations is very good.

The other curves in figure 10 show the same calculation procedure, but including medium corrections for the nucleon-nucleon cross section. The results are evidently very different than the previous ones. The dotted (dashed-dotted) [dashed] curves use phenomenological (Brueckner) [Pauli geometrical] recipes for medium effects on the cross sections. Based on the large error bars and spread of the experimental data, it is hard to judge what model adopted for medium corrections yields the best agreement with the data. It is clear that the inclusion of medium effects change the results to yield a closer reproduction of the data.

These findings are in agreement with our present understanding of medium modifications of the reaction cross sections and of several other reaction channels involving heavy ion scattering at intermediate energies ($\sim$ 50 MeV/nucleon).

IV. CONCLUSIONS

Often neglected effects, such as medium modifications of the nucleon-nucleon cross sections and Coulomb distortion, modify appreciably the nucleon knockout cross sections. As we have shown, these effects do not lead to an appreciable modification of the shapes of momentum distributions. This is explained by the fact that the momentum distributions are largely the Fourier transforms of the contributing parts of the single-particle wavefunctions, overwhelmingly their asymptotic regions, which are the Whittaker functions for protons or the Hankel functions for neutrons, sensitive only to the orbital momentum and the nucleon binding energies. We have shown these features explicitly by comparing our results with a large number of available experimental data. As expected on physics grounds, these corrections are larger for experiments at lower energies, around 50 MeV/nucleon, and for heavy targets.

As more experiments make use of heavier targets, it is worthwhile to illustrate the relevance of Coulomb corrections. Medium effects in knockout reactions have also been frequently ignored in the past. We show that they also have to be included in order to obtain a better accuracy of the extracted spectroscopic factors. Although these conclusions might not come as a big surprise, they have not been properly included in many previous experimental analyses.

[1] C.A. Bertulani and K.W. McVoy, Phys. Rev. C 46 (1992) 2638.
[2] P. G. Hansen, Nature 334 (1998) 194.
[3] J. A. Tostevin, J. Phys. G 25 (1999) 735.
[4] P. G. Hansen and J. A. Tostevin, Annu. Rev. Nucl. Part. Sci. 53 (2003) 219.
[5] A. Gade, P. Adrich, D. Bazin, M. D. Bowen, B. A. Brown, C. M. Campbell, J. M. Cook, T. Glasmacher, P. G. Hansen, K. Hosier, S. McDaniel, D. McGlinchery, A. Obertelli, K. Siwek, L. A. Riley, J. A. Tostevin, D. Weisshaar, Phys. Rev. C 77 (2008) 044306.
[6] L. Trache, F. Carstoiu, C.A. Gagliardi, and R.E. Tribble, Phys. Rev. Lett. 87, 271102 (2001).
[7] L. Trache, F. Carstoiu, A.M. Mukhamedzhanov, and R.E. Tribble, Phys. Rev. C 66, 035801 (2002).
[8] P. Navratil, C.A. Bertulani and E. Caurier, Phys. Rev. C 73, 065801 (2006).
[9] A.Banu *et al.*, Phys. Rev. C 84, 015803 (2011).
[10] L. Trache, F. Carstoiu, C.A. Gagliardi, and R.E. Tribble, Phys. Rev. C 69, 032802(R) (2004).
[11] C.A. Bertulani and P.G. Hansen, Phys. Rev. C 70, 034609 (2004).
[12] B. Abu-Ibrahim and Y. Suzuki, Phys. Rev. C 61, 051601 (R) (2000).
[13] B. Abu-Ibrahim, Y. Ogawa, Y. Suzuki, and I. Tanihata, Comp. Phys. Comm. 151, 369 (2003).
[14] J. A. Tostevin and B. A. Brown, Phys. Rev. C 74 (2006) 064604.
[15] E. C. Simpson, J. A. Tostevin, D. Bazin, B. A. Brown and A. Gade, Phys. Rev. Lett. 102 (2009) 132502.
[16] E. C. Simpson, J. A. Tostevin, D. Bazin, and A. Gade, Phys. Rev. C 79 (2009) 064621.
[17] L. Ray, Phys. Rev. C 20, 1857 (1979).
[18] M.S. Hussein, R.A. Rego and C.A. Bertulani, Phys. Rep. 201 (1991) 279.
[19] C.A. Bertulani and C. De Conti, Phys. Rev. C 81, 064603 (2010).
[20] G. Q. Li and R. Machleidt, Phys. Rev. C 48, 1702 (1993).
[21] G. Q. Li and R. Machleidt, Phys. Rev. C 49, 566 (1994).
[22] Cai Xiangzhou, Feng Jun, Shen Wenqing, Ma Yugang, Wang Jiansong, and Ye Wei, Phys. Rev. C58, 572 (1998).
[23] S. K. Charagi and S. K. Gupta, Phys. Rev. C 41, 1610 (1990).
[24] M.S. Hussein, K.W. McVoy, Nucl. Phys. A 445, 124 (1985).
[25] K. Hencken, G. Bertsch and H. Esbensen, Phys. Rev. C54, (1996) 3043.
[26] H. De Vries, C. W. de Jager, and C. De Vries, Atomic Data and Nuclear Data Tables 36, 495 (1987).
[27] Dao T. Khoa, Phys. Rev. C63, (2001) 034007.
[28] W.D Myers, Nucl. Phys. A 145, 387 (1970).
[29] G. Audi, A. H. Wapstra and C. Thibault, C, Nucl. Phys. A 729, 337 (2003).
[30] S. Goriely, M. Samyn, and J.M. Pearson, Phys. Rev. C75, 064312 (2007).
[31] I. Angeli, At. Data Nucl. Data Tables 87, 185 (2004).
[32] G. R. Satchler and W. G. Love, Phys. Rep. 55, 183 (1979).
[33] C.A. Bertulani and A. Gade, Comp. Phys. Comm. 175 (2006) 372.
[34] H. Jeppesen *et al.*, Nucl. Phys. A 739, 57 (2004).
[35] J.-L. Lecouey *et al.*, Phys. Lett. B 672, 6 (2009).
[36] E.K. Warburton and B.A. Brown, Phys. Rev. C 46, 923 (1992).
[37] A. Gade *et al.*, Phys. Rev. Lett. 93, 042501 (2004).
[38] C.A. Bertulani and G. Baur, Nucl. Phys. A 480, 615 (1988).
[39] T. Aumann *et al.*, Phys. Rev. Lett. 84 (2000) 35.
[40] R. Kanungo *et al.*, Phys. Rev. Lett. 102, 152501 (2009).
[41] Y. Ogawa, Y. Suzuki, and K. Yabana, Nucl. Phys. A 571, 784 (1994).
[42] W.D. Myers and W.J. Swiatecki, Ann. Phys. 55, 395 (1969); 186 (1974).
[43] R. Kanungo *et al.*, Physics Letters B 685, 253 (2010).
[44] R. F. Carlson, At. Data Nucl. Data Tables 63, 93 (1996).
[45] S. John, L.W. Townsend, J.W. Wilson, and R.K. Tripathi, Phys. Rev. C 48, 766 (1993).
[46] M. Beiner and R.J. Lombard, Ann. Phys. N.Y. 86, 262 (1974); F. Carstoiu and R.J. Lombard, ibid. 217, 279 (1992).
[47] http://www.nscl.msu.edu/∼brown/resources/resources.html
[48] L. Trache, F. Carstoiu, A. M. Mukhamedzhanov, and R. E. Tribble, Phys. Rev. C 66, 035801 (2002).